Detailed Kinetics of Titanium Nitride Synthesis

Hilmar Rode and Vladimir Hlavacek
Lab. for Ceramic and Reaction Engineering, Dept. of Chemical Engineering, State University of New York at Buffalo, Buffalo, NY 14260

A thermogravimetric analyzer is used to study the synthesis of TiN from Ti powder over a wide range of temperature, conversion and heating rate, and for two Ti precursor powders with different morphologies. Conversions to TiN up to 99% are obtained with negligible oxygen contamination. Nonisothermal initial rate and isothermal data are used in a nonlinear least-squares minimization to determine the most appropriate rate law. The logarithmic rate law offers an excellent agreement between the experimental and calculated conversions to TiN and can predict afterburning, which is an important experimentally observed phenomenon. Due to the form of the logarithmic rate law, the observed activation energy is a function of effective particle size, extent of conversion, and temperature even when the intrinsic activation energy remains constant. This aspect explains discrepancies among activation energies obtained in previous studies. The frequently used sedimentation particle size is a poor measure of the powder reactivity. The BET surface area indicates the powder reactivity much better.

Introduction

The synthesis of ceramic powders by self-propagating high-temperature synthesis (SHS) has reached the stage where it can be described as an established technology (Merzhanov, 1990). Several combustion systems have been extensively characterized (Agrafiotis, 1991; Kumar, 1988; Munir and Anselmi-Tamburini, 1989), and significant experimental and theoretical experience has been accumulated to scale up these processes. SHS has reached the point where many syntheses can be accomplished routinely. Yet there is still a relatively weak understanding of morphological aspects, which play a paramount role in determining the appeal of combustion as synthesis route and therefore need to be understood. Both in modeling (cf. Dandekar et al., 1990a,b) and experimentation (cf. Agrafiotis et al., 1991a), investigators have focused on propagation phenomena. Most studies which have addressed mechanistic issues (cf. Deevi and Munir, 1990; Eslamloo-Grami and Munir, 1990a) and the effect of powder morphology (Agrafiotis et al., 1991b) have not stressed the importance of a detailed characterization of the precursor powders.

Sufficient care has not been exercised to separate the intrinsic single-particle kinetics from global effects. The point was recently demonstrated by Pigeon and Varma (1993) who studied the kinetics of Si_3N_4 synthesis in great detail. Titanium nitride, which is efficiently synthesized by SHS, is a modern refractory ceramic with applications within the cutting tool and abrasives industry. It is also used as a composite ceramic with Si_3N_4 (cf. Shih and Yang, 1990). The synthesis of TiN has been well studied, and activation energies have been obtained by several investigators (cf. Agrafiotis et al., 1991a; Hirao et al., 1988; Eslamloo-Grami and Munir, 1990b). Their reported values for the activation energy differ greatly. In addition, the kinetic model used to evaluate the activation energies was not reported in all cases. Important questions remain unanswered regarding details pertaining to combustion synthesis, and the synthesis of TiN in particular, and a need exists for the experimental as well as theoretical investigation of such systems on a more fundamental level.

The major objective of this study is to understand better the synthesis of *TiN* by finding the *intrinsic* kinetics. Such kinetics should remain valid, even when system parameters such as conversion, temperature, powder morphology, and heating rate are varied over a wide range. Secondary objectives are to provide the practitioner with a matrix of high-quality conversion vs. time curves to be used for design purposes, and to provide a detailed and consistent rate expression for next-

Correspondence concerning this article should be addressed to H. Rode.

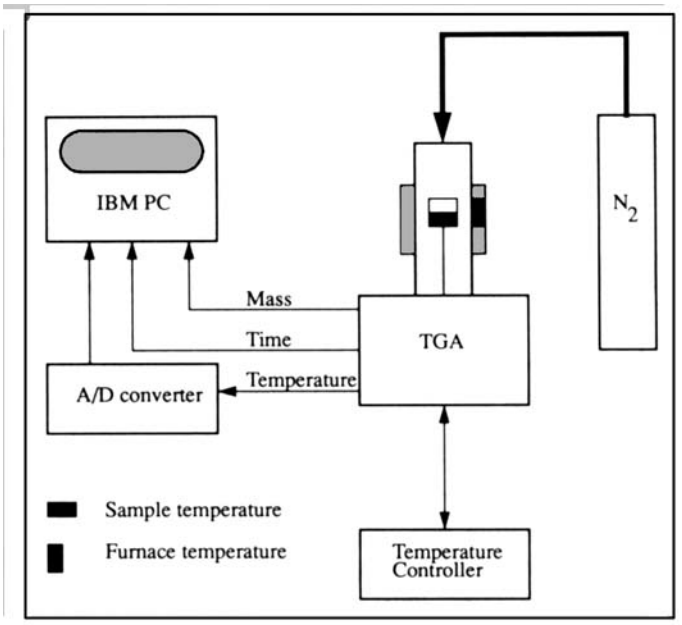

Figure 1. Experimental configuration.

generation modeling efforts capturing the essential features of SHS and combustion synthesis processes such as so-called *afterburning*. This is defined as a period after the combustion wave has passed through the sample when the conversion to product is still taking place at a significant, measurable rate, although much slower than during the passage of the combustion front.

Experimental Setup and Procedure

A diagram of the experimental configuration is shown in Figure 1. A thermogravimetric analyzer (TGA) (model ST-736, Harrop Industries, Columbus, OH) was used as the central instrument in this study. The unit has a maximum readability of 100 μg. It has a range of 20 to 1,600°C, a maximum heating rate of 30°C/min, and functions under atmospheric pressure. Care was taken to ensure that the mass recorded from the TGA was accurate: for each experiment a calibration was conducted to compensate for variations that occurred in the mass signal due to weight variations in components of the TGA setup and momentum effects on the crucible due to the temperature changes experienced by the nitrogen gas in the reaction tube. The nitrogen uptakes measured by the TGA were further checked by means of an oxygen/nitrogen determinator and through measurement of the sample mass before and after the experiment on an analytical balance (model 200 analytic balance, Sartorius Corporation, Long Island, NY). Excellent agreement was obtained. Temperature control and constant rate heating of the TGA furnace (cf. Figure 1) were achieved through a programmable unit with PID temperature control (model 2050, West Instruments, Schiller Park, IL). An A/D converter board (model 2801, Data Translation Inc., Marlboro, MA) was used to convert the analog temperature signal to digital format, whereas the mass signal was already digital and could be transferred to the computer directly by means of a serial port. Using data acquisition software, the two signals were accessed and then stored on a computer. In order to prevent gas diffusional resistance, experiments were conducted in a pure nitrogen atmosphere (cf. Glassman and Law, 1991).

Two different Ti powders were tested: Ti sponge powder (Nisso), −100 mesh, 99.8% purity from Metallwerk Plansee, Reutte, Austria and Ti sponge fines powder (Micron), −325 mesh, 99.4% purity from Micron Metals, Salt Lake City, UT. Prepurified nitrogen, minimum purity 99.998%, $O_2 < 5$ ppm, $H_2O < 3$ ppm from Cryogenic Supply, Buffalo, NY was used as the gas supply. Sample sizes ranging from 0.5 to 3.0 g were used, the upper limit being imposed by the volume of the crucible. The samples were not compacted, but used in the "as poured" densities, which were, as a percentage of theoretical density: 36% for the Nisso powder and 41% for the Micron powder. This is consistent with the recent trend (cf. Agrafiotis et al., 1991a,b) not to use compacted powder specimens, because the higher permeability of powders used in the "as poured" density offers distinct synthesis advantages. After placing the sample in the inert Al_2O_3 crucible within the reaction tube, the reaction tube was purged for 10 min. Then the data acquisition was initiated at a frequency of 10 s/sample and constant rate heating commenced, at rates varying between 10 and 30°C/min. The three signals recorded were the exact mass of the Ti powder in the crucible, the sample temperature, and the time. Once the desired temperature was reached after a period of constant rate heating, the temperature soak period commenced. Heating rates of 10, 20, and 30°C/min were used, and isotherms were obtained at TGA furnace temperatures of 1,000, 1,300, and 1,600°C. It should be emphasized that each experiment consisted of two distinct regimes: a nonisothermal heatup regime from 20°C to the temperature of the isotherm (1,000, 1,300 or 1,600°C), and a subsequent isothermal regime. Conversion of Ti to TiN took place during both nonisothermal and isothermal regimes. This complicated the data analysis, but provided a much stronger data set because nonisothermal and isothermal regimes tend to give different information concerning a suitable rate expression. The whole concept is demonstrated graphically in Figures 4 and 5. The black circles on the conversion profiles signify exactly where the isothermal regime starts for a particular experiment. The nitrogen flow rate was set to 0.9 l/min, providing an approximately stagnant, pure gaseous environment around the sample, which at the same time prevented ambient oxygen from entering the system due to back diffusion (the gas entered the reaction tube at the top and flowed out at the bottom). Copper turnings from Leco Corporation (St. Joseph, MI) were placed at the top of the reaction tube far enough away from the heating elements that the melting point of copper (1,083°C) was not exceeded. This had a twofold purpose: the turnings acted as a flow distributor, and as an oxygen scavenger to purify the incoming nitrogen.

Oxygen and nitrogen analyses were performed on an oxygen/nitrogen determinator (model TC-436, LECO Corporation, St. Joseph, MI). The particle sizes and morphologies were characterized by three measurements: sedimentation particle size analysis (model CAPA-700, Horiba Instruments Inc., Irvine, CA), BET surface area (model 2300, Micromeritics Instrument Corporation, Norcross, GA) and SEM (model S-800, Hitachi, Gaithersburg, MD). XRD (X-ray diffraction) was performed on representative samples using a powder diffractometer (model Nicolet with STOE data acquisition, Philips, Mahwah, NJ).

A summary of the relevant powder characteristics is provided

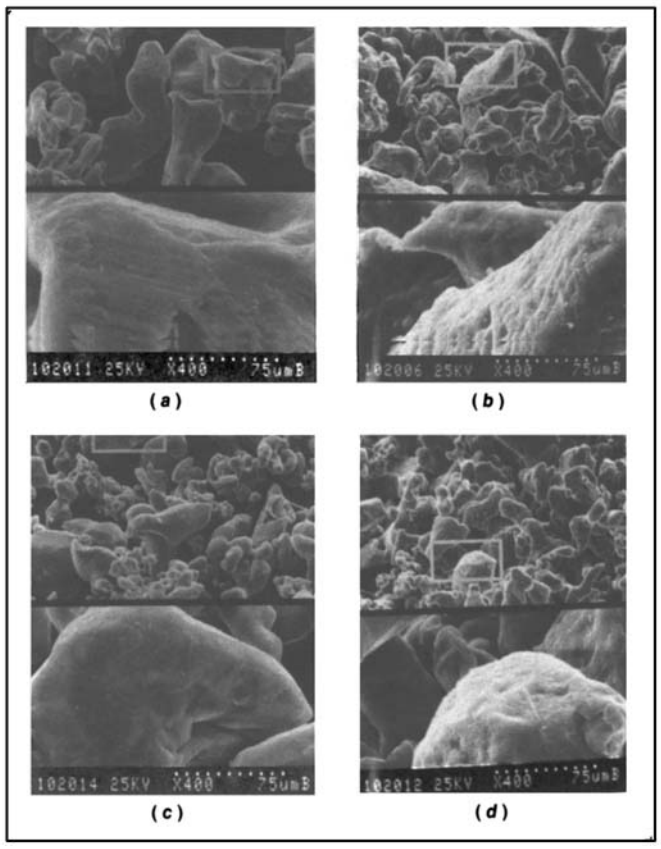

Figure 2. SEM micrographs of powders.

(a) Nisso Ti powder; (b) Nisso TiN product powder; (c) Micron Ti powder; (d) Micron TiN product powder.

in Table 1 and the SEM micrographs of the Ti precursor powders and the respective TiN product powders are shown in Figure 2. The average sedimentation particle-size radii (r_p) for the Nisso and Micron powders were 34 and 12 μm, respectively in contrast to the effective radii (r_e) calculated from the BET surface area measurement of 6.67 and 4.76 μm, respectively.

Theory

The experimental program was governed by four major features which are described in the following subsections.

Pure gas-solid system

Our equipment has an upper temperature limit of 1,600°C, which is below the melting point of both Ti and TiN. Thus the system is of a gas-solid nature. Typical reaction temperatures under combustion synthesis conditions reach 2,200 to 2,400°C which exceeds the melting point of Ti metal, yet the TiN product looks like the Ti precursor (cf. Agrafiotis et al., 1991a) even when the melting point of the precursor metal is severely exceeded. Eslamloo-Grami and Munir (1990b) also found negligible melting of Ti when sufficient dilution with TiN product was used. The lack of melting is due to dilution of the precursor metal powder by inert TiN product which lowers the adiabatic temperature rise of the reaction system and the fact that the temperature rise is coupled to conversion, that is, by the time the powder exceeds the Ti melting point, it has already been converted to a highly nonstoichiometric TiN product (Wriedt and Murray (1990) reported that TiN has a wide range of stoichiometry, existing approximately over the range $TiN_{0.42}$ to TiN). Therefore, we propose that this work should be applicable to experiments conducted under combustion synthesis conditions.

TiN: only product phase

This assumption is in agreement with the recent in-situ XRD work conducted by Merzhanov and his coworkers (cf. Khomenko et al., 1993). It is also in agreement with our XRD observations where only the TiN product phase was observed for experiments conducted at 1,300 and 1,600°C. For experiments conducted at 1,000°C, TiN was the major product phase, but in addition Ti_2N was observed as a minor product phase. Rode and Hlavacek (1993) also obtained Ti_2N XRD

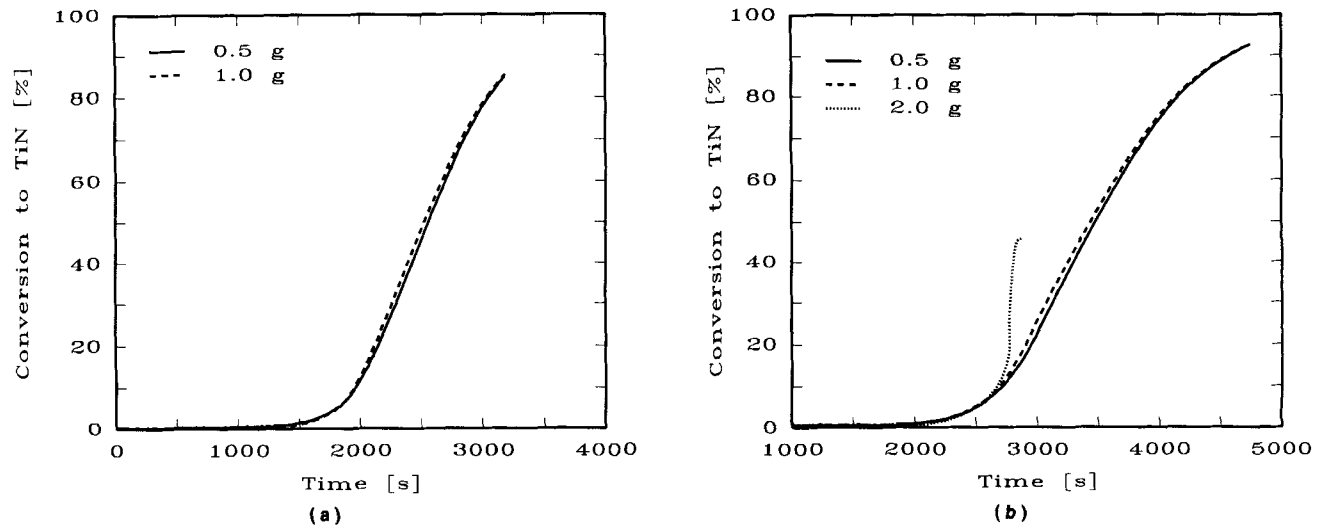

Figure 3. External mass-transfer limitations.

(a) Conversion to TiN vs. time for the Nisso powder at a heating rate of 30°C/min; (b) conversion to TiN vs. time for the Micron powder at a heating rate of 20°C/min.

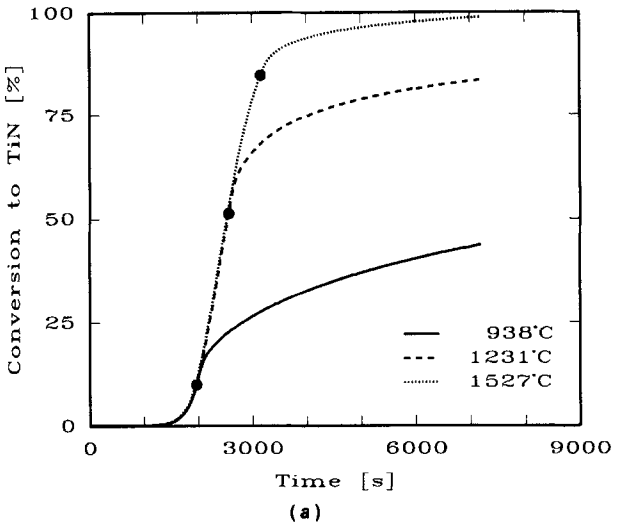

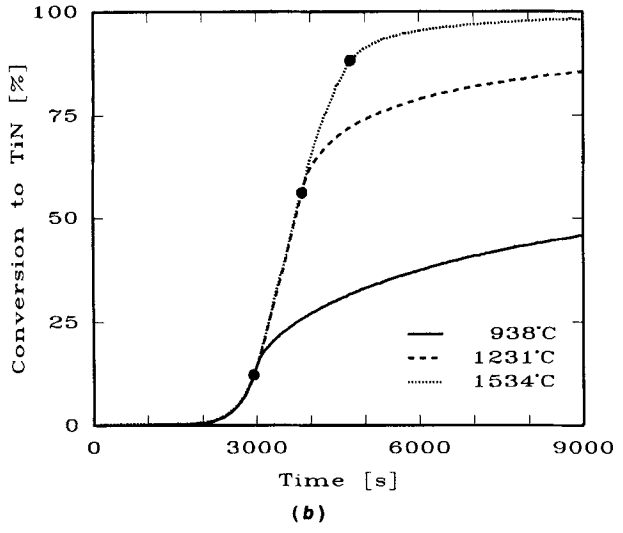

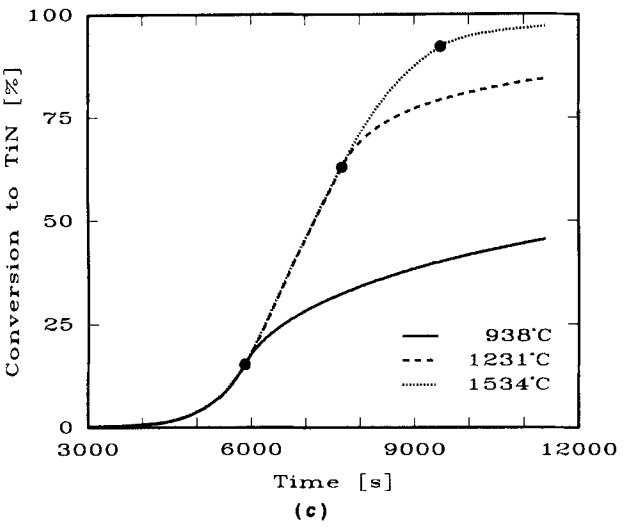

Figure 4. Experimental conversion to TiN vs. time for Nisso powder.

(a) 30°C/min; (b) 20°C/min; (c) 10°C/min.

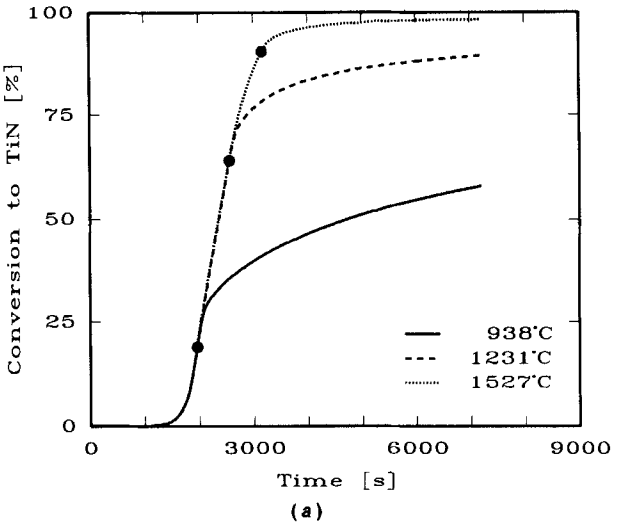

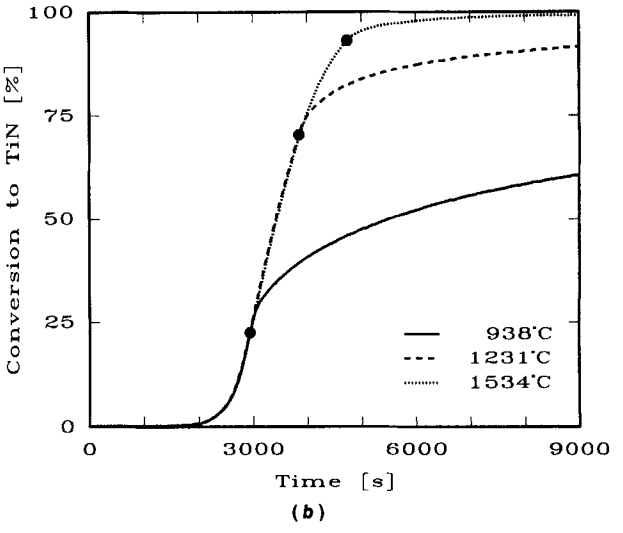

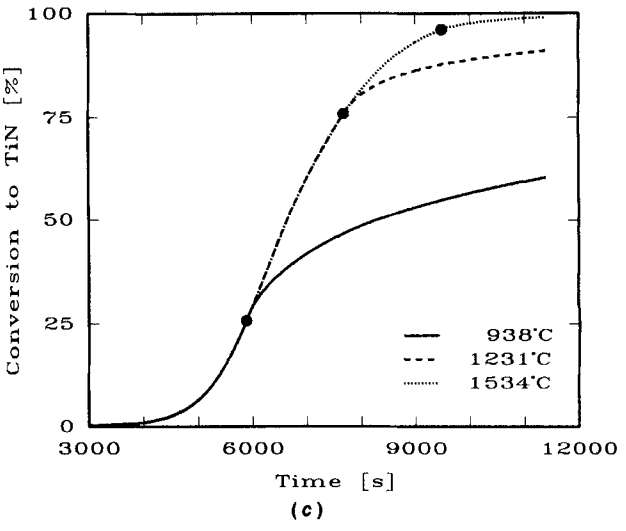

Figure 5. Experimental conversion to TiN vs. time for Micron powder.

(a) 30°C/min; (b) 20°C/min; (c) 10°C/min.

Table 1. Ti Powder Characterization

Powder	$r_p \times 10^6$ (m)	$r_e \times 10^6$ (m)	Oxygen (mass %)	Nitrogen (mass %)	BET (m^2/kg)
Nisso	34	6.67	0.070	0.003	100
Micron	12	4.76	0.120	0.005	140

peaks in Ti samples which were exposed to nitrogen at 600°C and contained approximately 5 mass % of nitrogen.

Rate-limiting sequential step

The sequential reaction steps for a nonporous particle undergoing a reaction of the type:

$$\text{gas} + \text{solid} \rightarrow \text{solid product}$$

where the gas is N_2, the solid precursor is Ti powder and the product is TiN powder, can be summarized as follows (cf. Szekely et al., 1976):

(1) External mass transfer of the gaseous reactant, N_2, from the bulk of the gas stream through the porous bed of Ti particles, to the surface of an individual solid particle. It should be emphasized that each individual particle is nonporous, and therefore this step does not refer to diffusion within the pores of an individual particle, but rather to diffusion of gas through the porous bed formed by the collection of Ti particles that form the reaction system. Should the reaction rate at the particle surface become too rapid compared to the maximum rate of diffusion of N_2 through the porous reaction bed, this diffusion would become rate limiting.

(2) Adsorption of N_2 at the solid surface.

(3) Transport of reactants through the TiN product layer.

(4) Chemical reaction to convert Ti to TiN.

To determine the intrinsic kinetics the reaction conditions were chosen such that external mass transfer through the porous bed did not control the overall reaction (steps 1 and 2). This entailed working with pure nitrogen and sufficiently small sample sizes. Under these conditions the reaction becomes independent of nitrogen pressure, as has been observed experimentally by Agrafiotis et al. (1991a) and Eslamloo-Grami and Munir (1990b). Several experiments were performed to ensure that mass-transfer restrictions through the porous bed were absent in the system, as shown in Figure 3. The conversion to TiN for the Nisso powder at a heating rate of 30°C/min is shown in Figure 3a for masses of 0.5 and 1.0 g, respectively. If mass-transfer limitations through the porous bed were present, we would expect the curve with the larger sample size to have a lower conversion. This is not the case. The sample with higher mass has a slightly higher conversion. This is due to the fact that the larger sample experienced a consistently higher temperature in the TGA reaction tube due to smaller relative heat losses compared to the exotherm released due to the reaction. The same curve is presented in Figure 3b for the micron powder at a heating rate of 20°C/min. For sample sizes of 0.5 and 1.0 g the conversion curves conform to the trend observed in Figure 3a. However, the 2.0 g sample size curve is dramatically different. At about 2,700 s (corresponds to 850 to 900°C), the conversion rises sharply and then slows down again. In this case the relative heat losses decreased sufficiently compared to the heat released by the exothermic reaction that the sample ignited. This led to a severe temperature rise and an accompanying increase in the rate of reaction. The temperature overshoot reached the melting point of Ti (1,660°C) and the sample melted. At this point the permeability to gas transfer decreased rapidly, and the reaction rate started to drop again. This explains the drop in the reaction rate observed after the steep rise in conversion.

Experiments were also performed using Ti precursor powder diluted by TiN product powder. The conversion achieved was the same as when pure Ti powder was used, indicating that mass-transfer limitations through the porous bed were absent. From these experiments it was decided to perform the kinetic measurements with a sample size of 1.0 g in all cases: smaller sample sizes could introduce larger experimental error, while larger sample sizes (cf. Figure 3b) could lead to ignition and uncontrolled conditions like melting which are not conducive to good kinetic measurements. It is also important to notice that the experiments performed to obtain data from which the kinetic parameters could be extracted were performed in the *kinetic* regime. Yet the factor which prevented ignition, that is, transition to the *combustion* regime, was not mass-transfer limitations through the porous bed or too slow heating rates, but high relative heat losses, which did not allow the occurrence of significant temperature overshoots.

Form of kinetic rate law

A typical rate law for a gas-solid reaction in terms of conversion, X, can be described by:

$$\frac{dX}{dt} = F[r_p]G[X]k_o e^{-E/RT} \tag{1}$$

where F and G represent functions of the particle size and conversion, respectively. SHS syntheses have high heats of reaction and activation energies. This has led researchers to believe that the feature of overriding importance in the rate law is the exponential term containing the activation energy in an Arrhenius temperature dependence. The part of the rate law dependent on the extent of conversion, $G[X]$, has often been discounted as unimportant. $G[X]$ is generally a semi-empirical relation derived from a fundamental mechanism. It can take several forms that are functionally diverse, and dependent upon different assumptions. Isothermal experiments where X is varied over time tend to give information regarding the form of $G[X]$ while experiments conducted at different temperatures elucidate the Arrhenius temperature dependence, that is, the value of the activation energy. A strength of the approach followed here is that nonisothermal data are also incorporated in the data analysis. In this work we show that whereas it is possible to match a variety of rate laws to experimental data over a limited parameter space, rate laws which are functionally deficient cannot match the experimental data over a wide parameter space.

Regardless of whether the reaction between the metal and oxidizing gas takes place in the slow oxidation regime or in the much faster combustion regime, the fundamental reaction steps which involve electronic and ionic transport through the product layer remain the same. For this reason we have used the well-studied oxidation field as a source for the selection of suitable rate laws. The most important rate laws used for

metal-gas reactions (cf. Kubaschewski and Hopkins, 1962) were all evaluated for suitability in this reaction system. The physical meaning which underpins each rate law is also discussed. The different rate laws can be interpreted using the generic form presented by Rozenband and Vaganova (1992) where δ represents the thickness of the product layer:

$$\frac{d\delta}{dt} = \delta^{-n} e^{-l\delta} k_o e^{-E/RT}. \tag{2}$$

Linear Law: $l=0$, $n=0$. The linear law states that the rate at which the product layer grows is independent of its thickness. Several explanations exist for this law:

(1) The overall reaction rate is limited by a surface reaction (cf. Fromhold, 1976).

(2) The overall reaction rate is limited by ion transfer in a self-generated electric field in the oxide (Cabrera-Mott or Grimley-Trapnell models) (cf. Kubaschewski and Hopkins, 1962).

(3) The overall reaction rate is limited by the diffusion of oxidizing gas through a porous scale (cf. Kubaschewski and Hopkins, 1962) due to spalling and cracking of the protective product layer.

Parabolic Law: $l=0$, $n=1$. The parabolic rate law is most often used to describe the oxidation of metals. The mechanism for the parabolic law was established by Wagner (1933). He proposed that the growth of the product layer is due to a concentration gradient. He realized that the film is composed of cations, anions, and electrons rather than neutral atoms, and the mechanism is based on the transport of these charged species rather than the transport of neutral atoms. Wagner assumed local equilibrium in the growing product layer, an assumption which does not always hold (cf. Fromhold, 1976). The parabolic law is almost equivalent in final functional form to the well-known shrinking core model (cf. Levenspiel, 1972) with diffusion through the product layer controlling, although the shrinking core model deals with the diffusion of neutral atoms rather than charged species.

Other derivations of the parabolic rate law are also possible (cf. Cabrera and Mott, 1949; Fromhold, 1976).

Cubic Law: $l=0$, $n=2$. The cubic rate law is less well founded theoretically than the other rate laws but is nevertheless used in the literature when other rate laws do not fit experimental data, and is therefore discussed here. Kubaschewski and Hopkins (1962) reported that this law is usually found as a transition; for example, it can be exhibited for thin films before the parabolic law is established.

Logarithmic Law: $l>0$, $n=0$. Several microscopic reaction steps can control the rate of conversion as the reaction proceeds, such as the outward transport of electrons through the product layer by tunneling, thermal emission or diffusion, or the transport of nitrogen ions to the reaction interface by electric field assisted diffusion (cf. Fromhold, 1976; Kubaschewski and Hopkins, 1962). Fromhold (1976) developed a consistent method to take all the microscopic reaction aspects into account by introducing a coupled currents approach to metal oxidation. It entails solving the equations that result when one permits the transport of charged species (cations, anions, and electrons) through the product layer while allowing transport due to concentration gradients and a convective type flux due to a self-generated electric field. The electric field is generated, because more rapidly moving charged particles leave behind charge of the opposite sign. This charge separation in the product layer represents an electric field within the film. It can also be called a coupled-currents approach because the ion and electron fluxes are both considered, and solved in a *consistent* way, that is, by preserving the overall charge neutrality of the particle. Kapila and Plawsky (1993) have recently used this kind of approach to model the oxidation of silver in integrated optical waveguide applications and obtained excellent agreement with experiments. Rode et al. (1992) used the coupled currents approach to model the initiation of combustion in metallic powders. The aim of this study is not to investigate the individual microscopic reaction steps, but rather to employ a *semiempirical* rate law which is relatively simple yet is consistent with the underlying reaction mechanism. The logarithmic law can be fitted empirically to the fundamental coupled-currents approach discussed in this section (cf. Cabrera and Mott, 1949; Kapila and Plawsky, 1993), and it is in this spirit that the logarithmic law is employed.

In order to convert Eq. 2 from product layer thickness, δ (not measurable), to conversion, X (measurable), it is necessary to make an assumption regarding the geometry and particle-size distribution of the particles. It is clear from the micrographs shown in Figure 2 that the particles are somewhat irregular in both cases. In addition there is a distribution of particle sizes. However, if we use a correct average particle size, it should be possible to quantify the reactivity of the powder with sufficient accuracy. Due to the irregularities of the powder particles, it is unsatisfactory to use the sedimentation particle size as a measure of such an average particle size which can be used to describe the reactivity. On the contrary, the reactivity should depend on the total surface area which is exposed to the environment. Therefore, a much better approximation than simply using the sedimentation particle size is to assume some idealized geometry (slab, cylinder, or sphere) and then to use the actual measured surface area to calculate an *effective* particle size, r_e. This approach, rather than using the sedimentation particle size, r_p, is also in agreement with the suggestions of Szekely et al. (1976) and the recent work on Si_3N_4 synthesis by Pigeon and Varma (1993).

Using the following relations, which assume a single effective particle size (that is, the particle size distribution is lumped) and spherical geometry:

$$r_e = \frac{3}{\rho \ \mathrm{BET}} \tag{3}$$

$$X = 1 - \left(\frac{r}{r_e}\right)^3 \tag{4}$$

$$\delta = r_e - r \tag{5}$$

we obtain:

$$\frac{dX}{dt} = \frac{3}{r_e^{1+n}} (1-X)^{2/3} \times [1-(1-X)^{1/3}]^{-n} \, e^{-lr_e[1-(1-X)^{1/3}]} \, k_o e^{-E/RT} \tag{6}$$

from Eq. 2. This conversion to an idealized spherical geometry

can also be performed easily for slab and cylindrical geometries.

Inspection of Eq. 6 reveals that the reaction has been considered irreversible. Munir and Holt (1987) have calculated equilibrium dissociation pressures for several nitrides. Their work indicates that it is indeed valid to assume irreversible kinetics for the Ti/TiN system. The Pilling-Bedworth ratio (ratio of product over precursor molar volume) for Ti/TiN is only 1.09 which allowed us to neglect expansion effects.

Once the experiments have been completed, the unknown parameters, l, n, k_o, and E can be determined through a nonlinear regression analysis. The different power laws require that n be varied discretely (0, 1, or 2), and therefore only integer values of n were allowed. A salient feature of the approach followed in this work is the assumption that the reaction can be described by a single rate law over a wide parameter space. In fact the rate limiting step can change during the course of the reaction.

Results and Discussion

Experimental results

The experimental results are presented in Figure 4 for the Nisso powder and in Figure 5 for the Micron powder as conversion to TiN against time. Each conversion curve consists of two regions: a nonisothermal, constant heating rate period, followed by a constant temperature soak regime. The TGA furnace temperature was set to 1,000, 1,300, and 1,600°C, respectively, to obtain the different isotherms, but due to heat losses from the sample crucible, the sample temperatures under isothermal conditions were somewhat lower, as indicated in Figures 4 and 5. Consider Figure 4a which shows the conversion of the Nisso Ti powder to TiN vs. time at a heating rate of 30°C/min. The solid line represents the experiment with an isotherm at 1,000°C. The transition from the nonisothermal regime (conducted at a heating rate of 30°C/min) to the subsequent isothermal regime is indicated by the solid circle. Notice that as soon as the temperature is held constant, the reaction rate starts to decrease markedly. The actual value of the sample temperature, 938°C, as indicated in Figure 4a, was lower than the TGA furnace temperature (1,000°C) due to heat losses. The other two curves contained in Figure 4a represent the conversions to TiN for experiments where the heating rate was also 30°C/min, but the isothermal regimes were initiated at a TGA furnace temperature of 1,300°C (1,231°C sample temperature) for the dashed line and 1,600°C (1,527°C sample temperature) for the dotted line.

The TGA furnace temperature was controlled accurately by the PID controller while the sample was heated indirectly by heat transfer (cf. Figure 1). Nevertheless, the sample heating rate was constant. In addition, because the sample temperature rather than the TGA furnace temperature was used for the calculation of the kinetic parameters, small deviations from constant rate heating were not important. The graphs at heating rates of 30, 20 and 10°C/min (Figures 4a–4c for the Nisso powder and Figures 5a–5c for the Micron powder) have been presented so that each graph represents a time passage of 6,000 s to facilitate comparisons between individual graphs. Note that at higher heating rates the reaction proceeds faster. Conversions were calculated on the basis of stoichiometric TiN being the only product phase present.

Figures 4 and 5 show that excellent reproducibility was obtained. High conversions were obtained up to 99% conversion to stoichiometric TiN in the case of the experiments that included an isotherm at 1,600°C. The conversions were verified by means of an oxygen/nitrogen determinator and through measurement of the sample before and after reaction on an analytical balance and quantitative agreement was obtained with the TGA measurement. It was also found that the product did not contain any significant oxygen impurities (important for purity as well as accuracy of conversion calculation). In the case of the Nisso powder, the oxygen content typically increased from 0.07% to 0.10%, while the corresponding increase for the Micron powder was from 0.12% to 0.14%. The product was a golden color typical of the cubic TiN phase. XRD was conducted on the both the Nisso and Micron TiN product powders after reaction at a heating rate of 20°C/min. Experiments which were conducted with isotherms at 1,000°C showed TiN as the major product phase and Ti_2N as the minor product phase. Experiments conducted with isotherms at 1,300 and 1,600°C, respectively, showed TiN to be the only product phase.

Thus two sets of conversion to TiN data for two significantly different Ti powders were obtained over a wide temperature and conversion range and for different heating rates. These were used to discriminate between the different rate laws.

Model discrimination and data fitting

The following data analysis procedure was used: for each powder the nine experimental conversion vs. time curves (1,000, 1,300 and 1,600°C × 10, 20 and 30°C/min) were appended to yield a composite data file which consisted of about 8,500 data points for each powder. This data file included both the nonisothermal and isothermal regimes, as discussed in Figures 4 and 5. Then a nonlinear least-squares optimization was used to fit the experimental conversions to the model-dependent calculated conversions. To calculate conversions the actual measured sample temperature, not the TGA furnace temperature (cf. Figure 1), was used. The quality of fit is summarized in Figure 6 for different rate laws for the Micron powder at a heating rate of 20°C/min. The linear law in Figure 6a is totally deficient, as could be intuitively expected. Of more interest is the parabolic law (similar to the shrinking core model) in Figure 6b. It provides a much better fit than the linear law, but is still functionally deficient. At higher conversions, especially at higher temperatures, the parabolic law overpredicts the conversion. A different fit might alleviate this problem, but that would introduce greater error elsewhere. This observation is important because the parabolic law (similar to the shrinking core model) has been widely used in these reaction systems to fit the experimental data.

This work which utilizes a much more demanding data set for the data fitting procedure than typically used—nonisothermal data, a large conversion span, different heating rates and powder morphologies, and perhaps most notably, a large temperature range—shows clearly that the parabolic law/shrinking core model description is inadequate. The cubic law (Figure 6c) provides a better overall fit than the parabolic law, but the same criticism can be brought against this law: it overpredicts the conversion to TiN significantly at higher temperatures and conversions. In addition, the cubic law is not

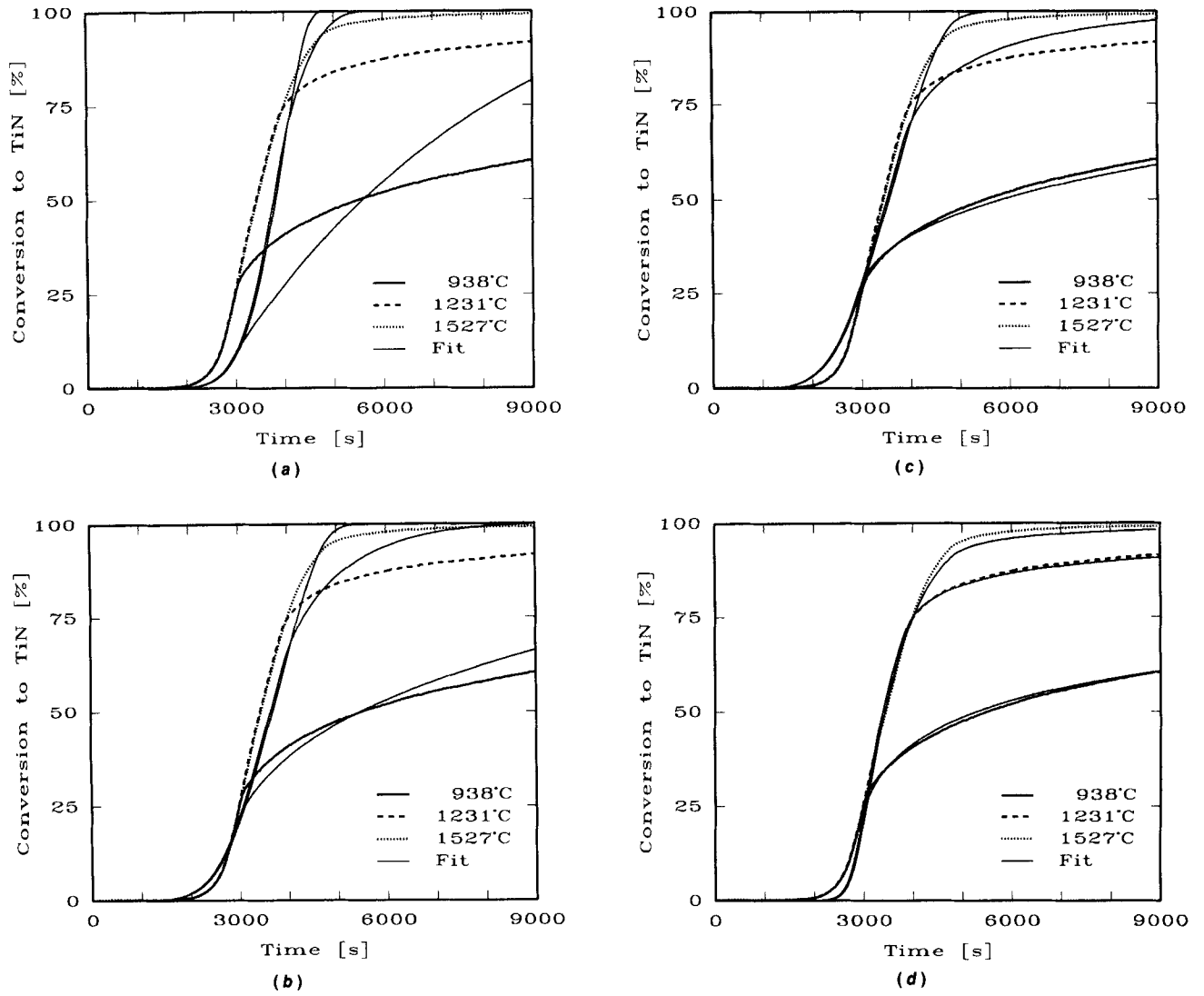

Figure 6. Comparison of data fit obtained for different rate laws for Micron Ti powder at 20°C/min.

(a) Linear law; (b) parabolic law; (c) cubic law; (d) logarithmic law.

theoretically as well founded as the other laws, which has to count against it. This common deficiency of the parabolic and cubic laws means that they cannot describe an important phenomenon which is experimentally observed during SHS, namely *afterburning*. The logarithmic rate law in Figure 6d provides a highly satisfactory description of the data. The deviations between the calculated and experimental conversions are small over the entire range of temperature and conversion, and perhaps more importantly, there are no diverging trends between the experimental and calculated conversions. At low conversion and temperature the logarithmic law somewhat overpredicts the conversion. Ti is known to dissolve N_2. In addition, Rode and Hlavacek (1993) observed Ti_2N through XRD measurements in powder Ti samples which were exposed to N_2 at 600 to 700°C. The Ti_2N phase was also observed in this study by XRD for low-temperature measurements. Thus it is possible that the higher experimental conversion at low temperatures is due to these factors.

The calculated rate constants for the different laws is summarized in Table 2. Note that for the power law rate expressions, that is, the linear, parabolic, and cubic laws, the calculated activation energies increase systematically as the exponent is increased. The fit between the logarithmic rate law and the experimental data is shown in Figure 7 for the Nisso powder and in Figure 8 for the Micron powder. Excellent agreement was obtained in all cases. We do not observe a diverging trend between the experimental and calculated conversions for any of the curves. Table 2 also shows that by taking the different particle size (6.67 and 4.76 μm, respectively for r_e, compared to 34 and 12 μm for r_p) into account consistently, we obtain kinetic parameters which are largely powder independent. The ratio of the two sedimentation particle sizes, r_p is 2.8, while this ratio is only 1.4 for the effective radii (r_e) calculated from the actual BET surface area measurements.

On the basis of these results, the family of power laws, that is, the linear, parabolic, and cubic rate laws are rejected in favor of the logarithmic law [Eq. 2 or Eq. 6 with $l>0$ and $n=0$, depending on whether product layer thickness (δ) or fractional conversion (X) is utilized]. The following average parameters which are based on the actual sample temperature

Table 2. Kinetic Parameters Calculated from Experimental Data for Different Laws

Powder	Δ (%)	r_{xy}	k_o (m^{1+n}/s)	E (kJ/mol)	l (1/m)	n
			Linear Rate Law			
Nisso	28.8	0.9794	1.42×10^{-6}	86		0
Micron	28.2	0.9801	3.09×10^{-6}	93		0
Together	26.6(N), 30.3(M)	0.9792	1.78×10^{-6}	88		0
			Parabolic Rate Law			
Nisson	14.8	0.9949	4.41×10^{-11}	127		1
Micron	14.1	0.9947	2.00×10^{-11}	118		1
Together	15.9(N), 14.0(M)	0.9947	2.98×10^{-11}	123		1
			Cubic Rate Law			
Nisso	6.8	0.9978	6.94×10^{-15}	184		2
Micron	7.5	0.9971	1.26×10^{-15}	165		2
Together	7.8(N), 8.1(M)	0.9973	3.21×10^{-15}	175		2
			Logarithmic Rate Law			
Nisso	5.8	0.9989	3.09×10^{-1}	198	1.91×10^{6}	
Micron	6.0	0.9993	9.33×10^{-1}	202	2.75×10^{6}	
Together	5.7(N), 9.0(M)	0.9978	5.94×10^{-1}	202	2.23×10^{6}	

(cf. Figure 1) are suggested for use. An effective particle size (r_e) which was determined from BET surface area measurements rather than the sedimentation particle size, r_p, was employed:

$$k_o[\text{m/s}]: \quad 5.94\times10^{-1}$$

$$E[\text{kJ/mol}]: \quad 202$$

$$l[1/\text{m}]: \quad 2.23\times10^{6}$$

Comparison to combustion synthesis conditions

It is instructive to analyze Eq. 6 and collect the terms from the two exponents. The one exponential term is due to the activation energy contained within a traditional Arrhenius temperature dependence. The second term arises due to the functionality of the logarithmic law. On this basis we can define an observed activation energy, E_{obs}, which is simply the sum of the two exponential terms:

$$E_{obs} = E + lr_eRT[1-(1-X)^{1/3}]. \tag{7}$$

Equation 7 suggests that the activation energy which will be observed *extrinsically* will depend on the *intrinsic* activation energy (E) as well as the temperature (T), the conversion (X), and the effective particle size (r_e). It should be stressed that the *intrinsic* activation energy, E, is indeed constant while the *extrinsic*, observed activation energy, E_{obs}, will be variable.

This has important implications for combustion synthesis and SHS. Experimental workers have long observed a so-called *afterburning* regime (cf. Eslamloo-Grami and Munir, 1990a; Agrafiotis et al., 1991a) for the Ti/N_2 as well as many other systems. It is a period after the combustion wave has passed through the sample when the conversion to the product is still taking place at a significant, measurable rate, although much slower than during the passage of the front. Calculated conversion to TiN profiles are presented in Figure 9 for the Micron powder at a heating rate of 1,000°C/s and a combustion temperature of 2,400°C, which represents combustion synthesis conditions (cf. Agrafiotis, 1991). The kinetic parameters used for the different rate expressions are those obtained from the least-squares optimization. The parabolic law is clearly deficient. The cubic law does a better job, although it does not exhibit a sharp reaction front and starts to overpredict conversion at 10 s (the same trend as was observed for the actual experiments, cf. Figure 6c), while the logarithmic law provides a curve which is entirely reasonable. The conversion is 50 to 70% at the passage of the front (defined as that instance where the temperature reaches its maximum), and the system exhibits an afterburning regime with a relatively slow approach to full conversion to the product.

The activation energy for the synthesis of TiN has been obtained by several investigators (cf. Agrafiotis et al., 1991b; Eslamloo-Grami and Munir, 1990b; Hirao et al., 1988). A big discrepancy exists between the different values, as shown in Table 3. This study clearly demonstrates that the activation energy which is extracted from kinetic measurements is rate law dependent proving that the rate law which is selected is crucial. In addition, Eq. 7 shows that the observed activation energy can indeed be a variable quantity, dependent on temperature, conversion, and effective particle size. We show in Table 3 that as conversion, temperature, and particle size vary, the observed activation energy can span the entire range of activation energies reported in the literature even though the intrinsic activation energy of 202 kJ/mol was used in all cases.

Conclusions

In this study the kinetics of TiN synthesis were obtained experimentally over a wide temperature and conversion range for different heating rates and for significantly different powders. A key aspect of the study was the utilization of nonisothermal rate data in addition to the traditional isothermal rate data to determine kinetic parameters.

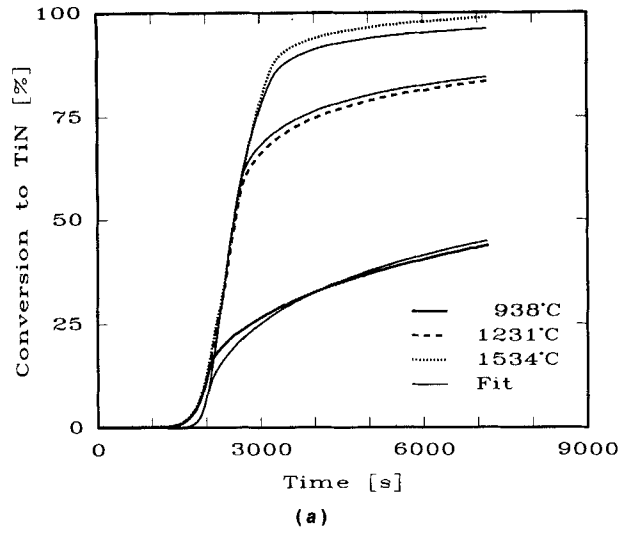

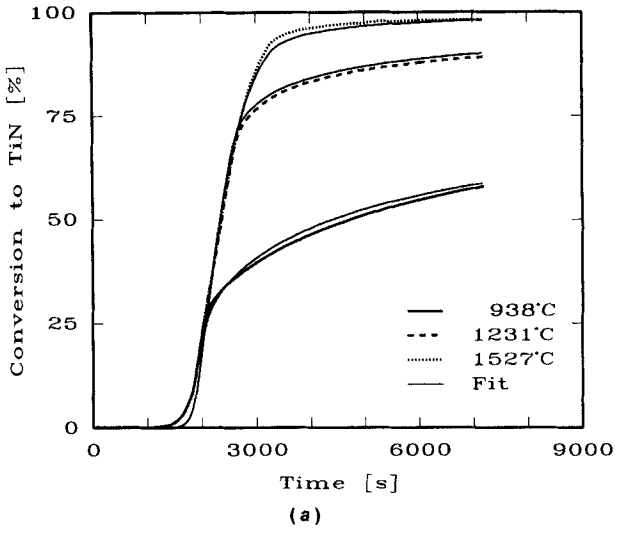

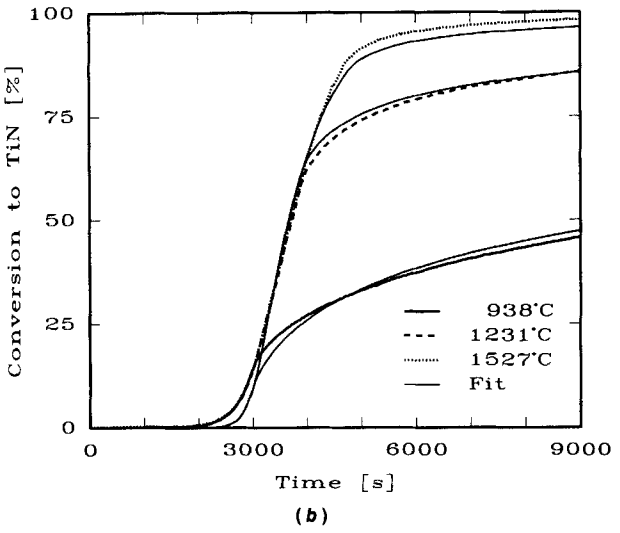

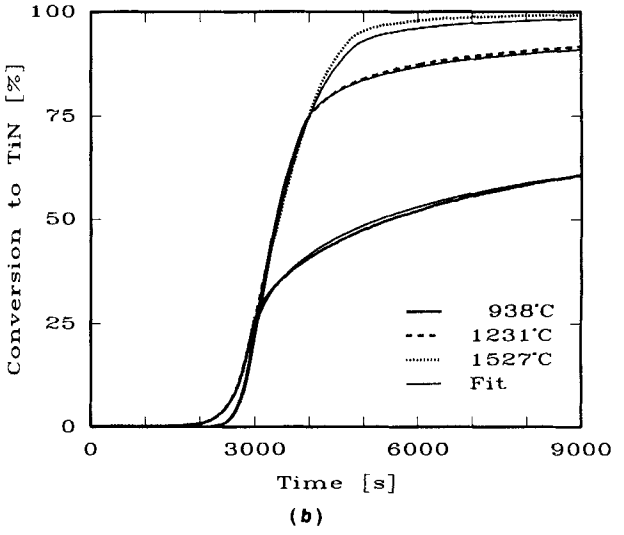

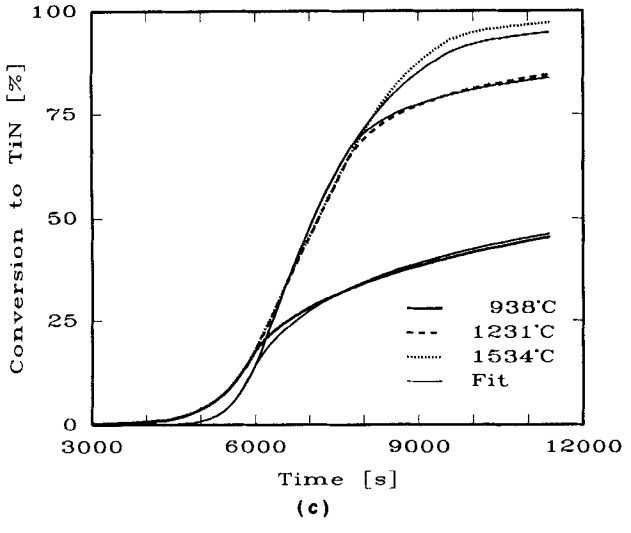

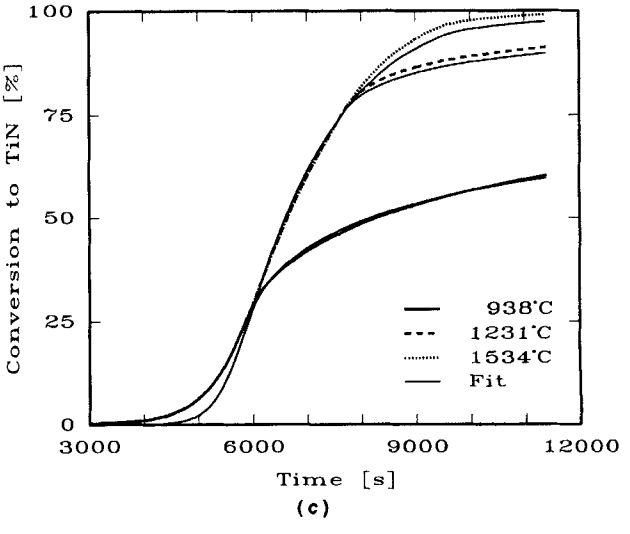

Figure 7. Fit between experimental and calculated conversions for Nisso Ti powder using the logarithmic law.

(a) 30°C/min; (b) 20°C/min; (c) 10°C/min.

Figure 8. Fit between experimental and calculated conversions for Micron Ti powder using the logarithmic law.

(a) 30°C/min; (b) 20°C/min; (c) 10°C/min.

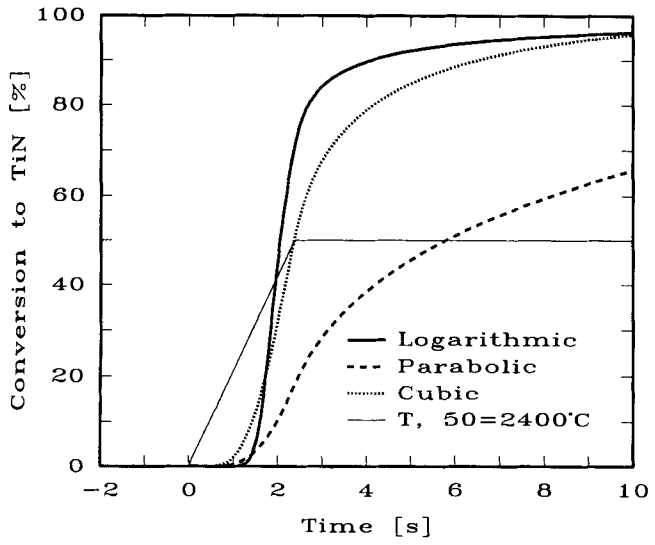

Figure 9. Calculated conversion to TiN vs. time for logarithmic, cubic and parabolic laws, and temperature vs. time.

Under SHS conditions for Micron Ti powder at a heating rate of 1,000°C/s.

Selection of the rate law plays an important role in the determination of the optimal data fit, a factor overlooked in previous investigations. The logarithmic law was selected as the rate law which is most suitable to represent this kind of reaction system over a wide range of parameters. This law can be described as a semiempirical rate law, which has its foundation in the fundamentally sound coupled currents approach taking the transport of ions and electrons through the product layer due to diffusion and a self-generated electric field into account. Due to the functionality of the logarithmic law, we showed that although the *intrinsic* activation energy, E, is a constant, the *extrinsically* observed activation energy, E_{obs}, is a function of the effective particle size (r_e), temperature (T) and extent of conversion (X). This allowed us to explain some of the discrepancies that exist between previous activation energies obtained for this reaction system by different investigators. The logarithmic rate law also allows a consistent explanation of *afterburning*, an important, experimentally observed phenomenon.

By conducting the study for two precursor powders with significantly different morphologies, we showed that sedimentation particle size is a poor measure of the powder reactivity, although used often. A much better measure of powder activity is provided by measuring the actual BET surface area and calculating an *effective* particle size based on an idealized geometry (slab, cylindrical, or spherical). Using the latter approach, kinetic parameters obtained for the different Ti powders were in excellent agreement. This suggests that if we take the effect of surface irregularities on powder reactivity into account consistently, it is possible to find a single reaction rate for powders with different morphologies.

This work provides conversion curves which can be used for design purposes by the practitioner. In addition, the logarithmic rate expression obtained here represents a great improvement for use in next generation modeling efforts, where it can supercede the first-order (with respect to conversion) kinetic law which has been used widely in modeling efforts.

Notation

BET = BET surface area of Ti powder, m^2/kg
E = activation energy for the reaction, kJ/mol
k_o = pre-exponential constant, m^{1+n}/s
l = coefficient in logarithmic law, 1/m
n = coefficient in rate law
r = radial position of the Ti/TiN interface, m
r_e = effective particle radius calculated from BET measurement, m
r_p = sedimentation particle size, radius, m
r_{xy} = correlation coefficient
R = gas constant, kJ/mol/K
t = time, s
T = temperature, K
X = fractional conversion

Greek letters

δ = product layer thickness, m
Δ = maximum deviation between experimental and calculated conversion, %
ρ = density of Ti metal, kg/m^3

Literature Cited

Agrafiotis, C. C., "Self-Propagating High-Temperature Synthesis of Nitrogen Ceramics," PhD Diss., State Univ. of New York, Buffalo (1991).

Agrafiotis, C. C., J. A. Puszynski, and V. Hlavacek, "Combustion Synthesis of Titanium and Tantalum Nitrides," *Combust. Sci. and Tech.*, **76**, 187 (1991a).

Agrafiotis, C. C., J. A. Puszynski, and V. Hlavacek, "Effect of Metal Particle Morphology on the Combustion of Refractory Metals in Nitrogen," *J. Am. Ceram. Soc.*, **74**, 2912 (1991b).

Cabrera, N., and N. F. Mott, "Theory of the Oxidation of Metals," *Rept. Prog. Phys.*, **12**, 163 (1949).

Deevi, S., and Z. A. Munir, "The Mechanism of Synthesis of Titanium Nitride by Self-Sustaining Reactions," *J. Mat. Res.*, **5**, 2177 (1990).

Dandekar, H. W., J. Degreve, J. A. Puszynski, and V. Hlavacek,

Table 3. Comparison of Kinetic Parameters to Previous Studies

Reference	Description	E_{obs} (kJ/mol)
This study	$r_e = 10\times10^{-6}$ m, $X=0.0$, $T=0$°C	202
This study	$r_e = 10\times10^{-6}$ m, $X=0.5$, $T=1{,}200$°C	266
This study	$r_e = 10\times10^{-6}$ m, $X=0.7$, $T=2{,}200$°C	354
This study	$r_e = 5\times10^{-6}$ m, $X=0.7$, $T=2{,}200$°C	278
Agrafiotis et al. (1991a)	$r_p = 15\times10^{-6}$ and 40×10^{-6} m	270
Hirao et al. (1988)	$r_p < 44\times10^{-6}$ m	370
Eslamloo-Grami and Munir (1990b)	$r_p = 10\times10^{-6}$ m	342

"Reaction Front Propagation Characteristics in Exothermic Noncatalytic Gas-solid Systems," *Chem. Eng. Comm.*, **92**, 199 (1990a).
Dandekar, H. W., J. A. Puszynski, and V. Hlavacek, "Two-Dimensional Numerical Study of Cross-Flow Filtration Combustion," *AIChE J.*, **36**, 1649 (1990b).
Eslamloo-Grami, M., and Z. A. Munir, "Effect of Porosity on the Combustion Synthesis of Titanium Nitride," *J. Am. Ceram. Soc.*, **73**, 1235 (1990a).
Eslamloo-Grami, M., and Z. A. Munir, "Effect of Nitrogen Pressure and Diluent Content on the Combustion Synthesis of Titanium Nitride," *J. Am. Ceram. Soc.*, **73**, 2222 (1990b).
Fromhold, A. T., *Theory of Metal Oxidation: I. Fundamentals*, North-Holland, New York (1976).
Glassman, I., and C. K. Law, "Sensitivity of Metal Reactivity to Gaseous Impurities in Oxygen Environments," *Combust. Sci. and Tech.*, **80**, 151 (1991).
Hirao, K., Y. Miyamoto, and M. Koizumi, "Reaction Analysis of the Combustion Syntheses of Transition Metal Nitrides," *Proc. Int. Inst. for Sci. of Sintering, Sintering*, **1**, 551 (1988).
Kapila, D., and J. L. Plawsky, "Solid-State Film Diffusion for the Production of Integrated Optical Waveguides," *AIChE J.*, **39**, 1186 (1993).
Khomenko, I. O., A. S. Mukasyan, V. I. Ponomaryev, I. P. Borovinskaya, and A. G. Merzhanov, "Dynamics of Phase Forming Processes in the Combustion of Metal-Gas Systems," *Comb. and Flame*, **92**, 201 (1993).
Kubaschewski, O., and B. E. Hopkins, *Oxidation of Metals and Alloys*, 2nd ed., Butterworths, London (1962).
Kumar, S., "Self-Propagating High Temperature Synthesis of Ceramic Materials," PhD Diss., State Univ. of New York, Buffalo (1988).
Levenspiel, O., *Chemical Reaction Engineering*, 2nd ed., Wiley, New York (1972).
Merzhanov, A. G., "Self-Propagating High-Temperature Synthesis: Twenty Years of Research and Findings," in *Combustion and Plasma Synthesis of High-Temperature Materials*, Z. A. Munir and J. B. Holt, eds., VCH Publishers, New York (1990).
Munir, Z. A., and V. Anselmi-Tamburini, "Self-Propagating Exothermic Reactions: The Synthesis of High Temperature Materials by Combustion," *Mat. Sci. Rep.*, **3**, 277 (1989).
Munir, Z. A., and J. B. Holt, "The Combustion Synthesis of Refractory Nitrides: I. Theoretical Analysis," *J. Mat. Sci.*, **22**, 710 (1987).
Pigeon, R. G., and A. Varma, "Quantitative Kinetic Analysis of Silicon Nitridation," *J. Mat. Sci.*, **28**, 2999 (1993).
Rode, H., and V. Hlavacek, "An Experimental Study of Titanium Powder Reactivity in Gaseous Environments: I. Oxidation," *Combust. Sci. and Tech.*, accepted (1993).
Rode, H., V. Hlavacek, H. J. Viljoen, and J. E. Gatica, "Combustion of Metallic Powders: A Phenomenological Model for the Initiation of Combustion," *Combust. Sci. and Tech.*, **88**, 153 (1992).
Rozenband, V. I., and N. I. Vaganova, "A Strength Model of Heterogeneous Ignition of Metal Particles," *Comb. and Flame*, **88**, 113 (1992).
Shih, C. J., J. M. Yang, and A. Ezis, "Feasibility Study of Developing an *In Situ* TiN-Reinforced Si_3N_4 Composite," *Scripta Metallurgica et Materialia*, **24**, 2419 (1990).
Szekely, J., J. W. Evans, and H. Y. Sohn, *Gas-Solid Reactions*, Academic Press, New York (1976).
Wagner, C., "Beitrag zur Theorie des Anlaufvorgangs," *Z. Physikal. Chem. B*, **21**, 25 (1933).
Wriedt, H. A., and J. L. Murray, *Binary Alloy Phase Diagrams*, T. B. Massalski, ed., Vol. 1, ASM, Materials Park, OH (1990).

Manuscript received Dec. 26, 1993, and revision received Feb. 22, 1994.